Structural dynamics of the GluK3-kainate receptor neurotransmitter binding domains revealed by cryo-EM

International Journal of Biological Macromolecules 149 (2020) 1051–1058

Contents lists available at ScienceDirect

International Journal of Biological Macromolecules

journal homepage: http://www.elsevier.com/locate/ijbiomac

Structural dynamics of the GluK3-kainate receptor neurotransmitter binding domains revealed by cryo-EM

Jyoti Kumari [a], Ameya D. Bendre [a], Sumedha Bhosale [b], Rajesh Vinnakota [a], Ananth P. Burada [a], Giancarlo Tria [c], Raimond B.G. Ravelli [c], Peter J. Peters [c], Manali Joshi [b], Janesh Kumar [a,*]

[a] Laboratory of Membrane Protein Biology, National Centre for Cell Science, NCCS Complex, S. P. Pune University, Pune, Maharashtra 411007, India
[b] Bioinformatics Centre, S. P. Pune University, Pune, Maharashtra 411007, India
[c] The Maastricht Multimodal Molecular Imaging Institute (M4I), Division of Nanoscopy, Maastricht University, PO Box 616, 6200 MD Maastricht, the Netherlands

ARTICLE INFO

Article history:
Received 26 November 2019
Received in revised form 28 January 2020
Accepted 28 January 2020
Available online 30 January 2020

Keywords:
Glutamate receptor
Cryo-electron microscopy
Kainate

ABSTRACT

Kainate receptors belong to the ionotropic glutamate receptor family and play critical roles in the regulation of synaptic networks. The kainate receptor subunit GluK3 has unique functional properties and contributes to presynaptic facilitation at the hippocampal mossy fiber synapses along with roles at the post-synapses. To gain structural insights into the unique functional properties and dynamics of GluK3 receptor, we imaged them *via* electron microscopy in the apo-state and in complex with either agonist kainate or antagonist UBP301. Our analysis of all the GluK3 full-length structures not only provides insights into the receptor transitions between desensitized and closed states but also reveals a "non-classical" conformation of neurotransmitter binding domain in the closed-state distinct from that observed in AMPA and other kainate receptor structures. We show by molecular dynamics simulations that Asp759 influences the stability of the LBD dimers and hence could be responsible for the observed conformational variability and dynamics of the GluK3 *via* electron microscopy. Lower dimer stability could explain faster desensitization and low agonist sensitivity of GluK3. In overview, our work helps to associate biochemistry and physiology of GluK3 receptors with their structural biology and offers structural insights into the unique functional properties of these atypical receptors.

1. Introduction

Kainate receptors (KARs) belong to the family of ionotropic glutamate receptors (iGluRs) that mediate the majority of excitatory postsynaptic potentials in the central nervous system (CNS) [1]. KARs assemble as tetramer and are abundantly expressed in the hippocampus and cerebellar region of the brain [2]. While the postsynaptic KARs are associated with excitatory neurotransmission, the presynaptic KARs have been reported to engage with inhibitory neurotransmission in the CNS [3,4]. The activation of KAR generates various forms of synaptic plasticity like Long Term Potentiation (LTP) and Long Term Depression (LTD) patterns that are considered to be associated with memory and learning [5]. Thus, the dysfunction of these receptors is linked to several CNS disorders such as schizophrenia, epilepsy, and Alzheimer's disease [6]. Despite sharing similarities in sequence, membrane regional anatomy, and organization of domains with other iGluRs, KARs possess distinct pharmaco-physiological properties [7] and hence are important targets for therapies of CNS disorders.

GluK3 is undoubtedly the most enigmatic member of the KAR family and contributes to presynaptic facilitation at hippocampal mossy fiber synapses [4,8]. These receptors have low sensitivity towards glutamate and thus fast desensitization kinetics. Besides, they also exhibit voltage-dependent block by intracellular spermine and are permeable to calcium ions [9]. They are also potentiated by zinc which acts as an endogenous allosteric modulator for native KARs containing GluK3 subunits [10]. These characteristics make GluK3 unique across the two families of AMPA and kainate receptors. Crystal structures of isolated LBD (Ligand Binding Domain) combined with elegant electrophysiology experiments have revealed the mechanisms of Zinc potentiation [10] and ligand-induced structural transitions in the context of isolated neurotransmitter binding domain [10] [11].

Similarly, ATD (Amino Terminal Domain) crystal structures shed light on its conserved 2-fold symmetric dimer-of-dimers assembly [12]. This tetrameric assembly was preserved in the full-length GluK3 receptor structures trapped in desensitized (SYM bound) and closed states (UBP310 bound) elucidated *via* cryo-EM. These structures

Abbreviations: AMPA, α-amino-3-hydroxy-5-methyl-4-isoxazolepropionic acid; ATD, Amino terminal domain; CHS, cholesterol hemisuccinate; COM, Center of mass; CTD, Carboxyl terminal domain; DDM, n-dodecyl-β-D-maltopyranoside; iGluR, ionotropic Glutamate Receptor; KAR, Kainate Receptor; LBD, Ligand binding domain; NMDA, *N*-methyl-D-aspartate.

* Corresponding author at: National Centre for Cell Science, NCCS Complex, S. P. Pune University Campus, Ganeshkhind, Pune 411007, India.
E-mail address: janesh@nccs.res.in (J. Kumar).

https://doi.org/10.1016/j.ijbiomac.2020.01.282
0141-8130/

established the similarity of the desensitized state in GluK3 and GluK2 receptors with LBD adopting a quasi-4-fold symmetry. However, the UBP310 bound structure is trapped in a non-classical closed-state, where only two LBD domains adopt the dimeric arrangement necessary for receptor activation, while the other two remain in a desensitized-like state [13]. This is in contrast to GluK2 or GluA2 where the antagonist binding leads to the classical closed state with two LBD dimers. To capture more intermediates in the gating cycle and investigate the structural dynamics of GluK3 receptors, we imaged them *via* electron microscopy in the apo state and in complex with either kainate (agonist) or UBP301 (antagonist). Analysis of the structures revealed distinct conformational states for both the agonist and the antagonist bound forms. Additionally, the apo state revealed conformational heterogeneity of the ligand-binding domains. Further, we show by molecular dynamics simulations that the residue Asp759, which is unique to GluK3 and is positioned at the LBD dimer interface, is crucial for the stability of LBD dimers and could be responsible for the observed conformational variability and dynamics of the GluK3 ligand-binding domains.

2. Results

2.1. Receptor purification and structure determination

Due to the poor yield and low stability, the wild type GluK3 was modified as mentioned in Section 2.2. The final construct named $GluK3_{EM}$, as shown in Fig. 1A was found to be most suitable for structural studies [13]. Optimization of receptor expression, purification and stabilization was carried out as detailed in Supplementary text and Supplementary Figs. S1 and S2. The functionality of the recombinant receptor was checked by electrophysiology. We observed that the fast application of glutamate and kainate evoked currents that were comparable in both wild type and $GluK3_{EM}$ using whole-cell patch clamp recordings in HEK293T cells. The peak amplitude ratios of I_{Glu}/I_{Kai} for wild type and $GluK3_{EM}$ were nearly identical, suggesting

Table 1
Electron microscopy data collection, refinement and validation statistics.

	GluK3-Kainate	GluK3-UBP301	GluK3-Apo
Data collection and processing			
Microscope	Tecnai Arctica	Tecnai Arctica	T12
Voltage (kV)	200	200	120
No. of micrographs	2845	2005	1215
Camera	Falcon 3	Falcon 3	Eagle
Mode of recording	Integrated mode	Integrated mode	Integrated mode
Exposure time (seconds)	3	3	3
Defocus range (μm)	1.0–3.5	1.0–3.5	1.5–3.5
Pixel size (Å)	0.935	1.27	3.5
Symmetry	C1	C1	C1
Initial particle images (no.)	491,250	118,670	39,912
Final particle images (no.)	46,106	24,997	15,217
Map resolution (Å)	9.6	10.6	–
FSC threshold	0.143	0.143	
Refinement			
Initial model used (PDB code)	6JFY	6JFY	–
Model resolution (Å)	8.9	11.4	–
FSC threshold	0.5	0.5	
Map-to model fit, CC_mask	0.83	0.80	
Model composition			–
Non-hydrogen atoms	23,017	22,965	
Protein residues	2881	2873	
RMSD			–
Bond lengths (Å)	0.005	0.008	
Bond angles (°)	1.039	1.082	
Validation			–
MolProbity score	1.99	2.07	
Clashscore	10.44	13.11	
Ramachandran plot			–
Favored (%)	92.91	93.15	
Allowed (%)	7.09	6.81	
Disallowed (%)	0.0	0.04	

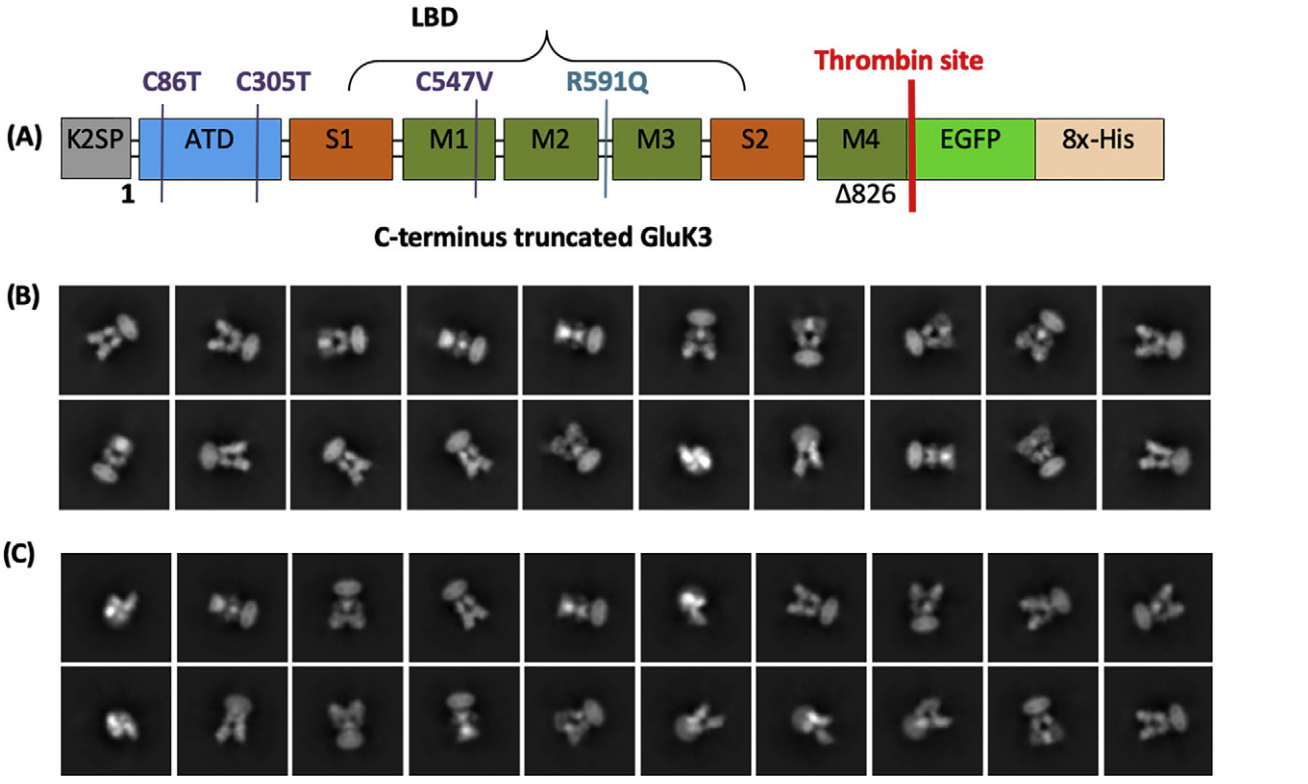

Fig. 1. Construct design and 2D classification (A) GluK3 was fluorescently tagged with EGFP for FSEC screening and octa-His tag for affinity purification at C-ter, three cysteine mutations were made, two in ATD and one in M1 helix as shown. Panels (B) and (C) show representative 2D classes for kainate and UBP301 bound form respectively.

that $GluK3_{EM}$ forms a functional channel when expressed in HEK293T cells and was similar to wild-type receptors. Our results are also consistent with previous electrophysiology reports which suggest that GluK3 has less sensitivity to glutamate and even lesser for kainate [14]. Similarly, we also tested the effect of antagonist UBP301. Although GluK3 LBD has a weak affinity for UBP301, we found that 100 μM UBP301 was enough to block glutamate evoked currents in both wild type and $GluK3_{EM}$ (Supplementary Fig. S3). To deduce the complete receptor structure, the receptor molecules were captured in the presence of 10 mM kainate to trap the desensitized state and 100 μM UBP301 to image the closed state using single-particle cryo-EM (Supplementary Fig. S4). The reference-free 2D classification showed that multiple orientations of receptors were trapped and sufficient for 3D map reconstruction and refinement (Fig. 1B and C and Supplementary Fig. S5). The data collection and refinement parameters are listed in Table 1.

2.2. The overall structure of GluK3

The 3D structure of GluK3 was determined by single-particle cryo-EM at a resolution of ~9.6 Å for kainate bound and ~10.6 Å for UBP301 bound state, estimated by the gold standard 0.143 Fourier shell correlation (FSC) criterion [15] and displays an overall architecture similar to structures of GluA2 and GluK2 receptors [16] [17] (Supplementary Figs. S6 and S7). Laterally, the tetramer appears 'Y' shaped, typical to the ionotropic glutamate family of receptors. The map clearly indicated the dimer of dimers arrangement at ATD two-fold symmetry mates. Also, the TM domains were arranged in 4-fold symmetry as observed in the model similar to previously reported structures (Fig. 2 and Supplementary Fig. S8).

2.3. Kainate and UBP301 bound GluK3 receptor

In both kainate and UBP301 bound states, the receptor consists of a 3-layered assembly of ATD, LBD, and TM regions, as seen earlier [18] [19]. In both structures, 2-fold symmetric ATDs and 4-fold symmetric TM domains were observed with the ATDs in typical N-shaped orientation (top view) (Fig. 2A, B, D and E). While the LBDs in kainate bound state mimic the quasi-4-fold arrangement representative of the desensitized state and reported in GluK3-SYM bound structure [13], the arrangement in antagonist UBP301 bound state is different. In the UBP310 complex reported earlier, two LBDs exist in a dimeric configuration, and the other two LBDs remain separated as in the desensitized state, whereas UBP301 bound state reveals a partially formed LBD dimer and desensitized like arrangement for the other two LBDs. Due to this arrangement, the partially formed LBD dimer (BC) does not maintain 2-fold symmetry observed earlier for GluK2-LY or GluK3-UBP310 complexes. (Supplementary Fig. S9A and B).

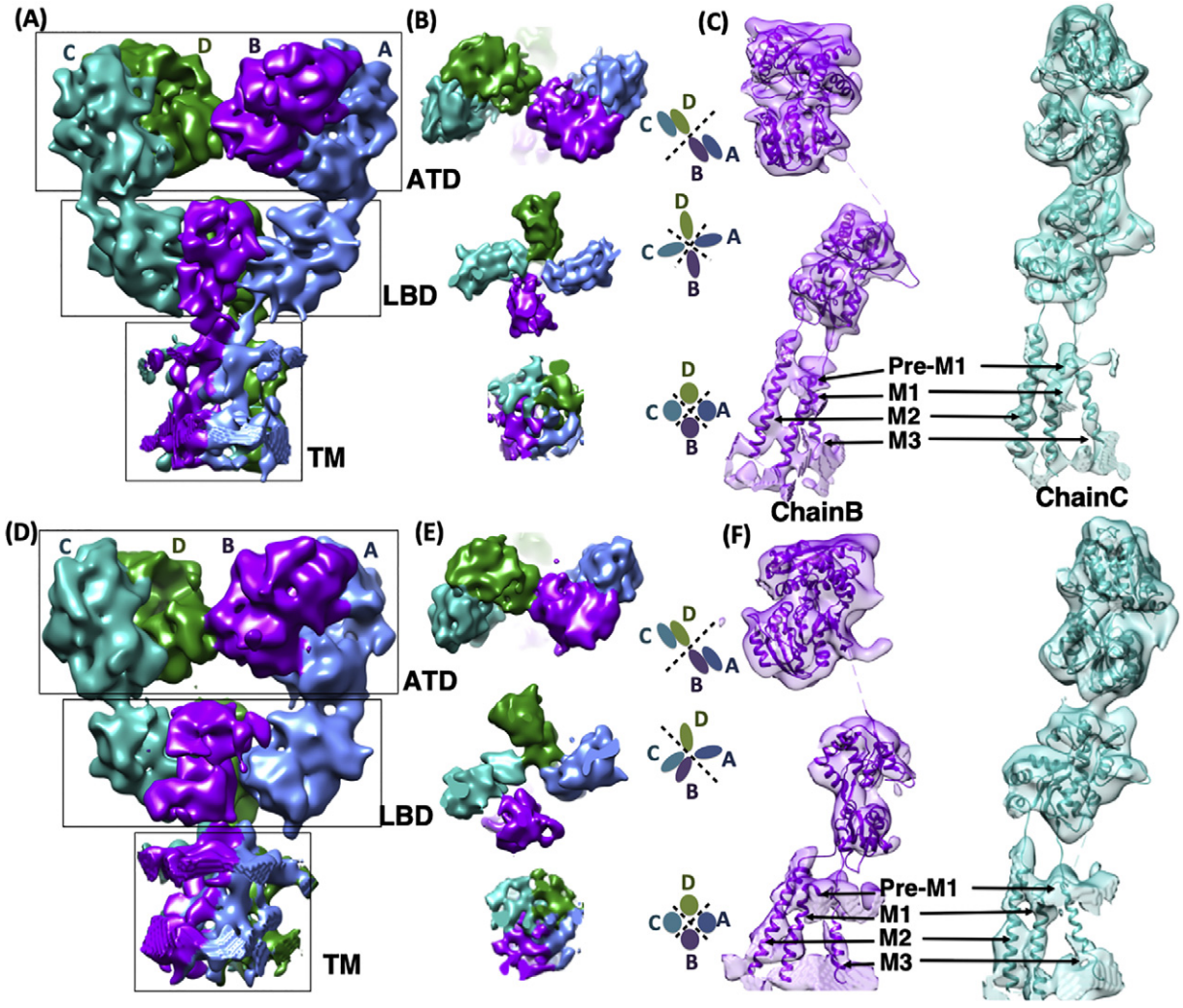

Fig. 2. GluK3 structure in Kainate and UBP301 bound states. Panels (A), (B), (C) show 3D EM map of GluK3 bound with Kainate while (D), (E), (F) panels show density map for UBP301 bound form. The regions corresponding to various domains ATD, LBD and TM (Pre-M1, M1, M3, and M4) are indicated. Panels A and D show the view of intact full-length receptors while panels B & E show the top views of extracellular ATD, LBD, and transmembrane TM domains. Subunit arrangement at the various domains is also represented in cartoon. Panels C & F show the segmented map of proximal subunit B and distal subunit C fitted with the refined model.

2.4. Conformational dynamics of the GluK3 LBD domain

To understand the underlying conformational changes in the LBD domains, we compared kainate and UBP301 bound structures with the recently reported SYM and UBP310 bound complex [13] (Supplementary Fig. S10). As expected, the LBD domains in agonist SYM and kainate complexes were very similar, and the LBD tetramers could be superimposed with a root mean square deviation (RMSD) of 1.7 Å for 998 Cα atoms. The receptor transition between the two states requires minor movements of the ligand binding domain (Fig. 3A and B). However, the transition from agonist kainate bound state to antagonist UBP301 bound state requires significantly larger rotational movements of the LBD domains apart from the opening up of the cleft due to binding of larger antagonist molecule. Owing to this, the RMSD for LBD tetramer superimposition between kainate and UBP301 bound states is ~12.1 Å for 992 Cα atoms. Consistent with this observation, the LBD-distal subunit B swings clockwise by ~113° in the horizontal plane, while the LBD-proximal subunit C rotates anticlockwise by ~10° to achieve a partial dimeric configuration distinct to that observed in UBP310 bound state (Fig. 3**A**). The LBD of subunits A and D undergo a smaller degree of anti-clockwise rotation by ~7° and ~10° respectively and hence remain in a desensitized-like-state (Fig. 3**A**). Due to this rearrangement, the distance between COMs of S1 domains of subunits B and C reduces by ~8 Å while for S2 domains it increases by ~5 Å (Fig. 3B). On the other hand, the separation between S1 and S2 COMs for subunits A and B increases by ~4 Å and 14 Å respectively. Additionally, the COMs (S1 lobe) of subunits B and C in UBP310 bound complex is closer by 6 Å coupled with ~6–7° rotation leading to a tighter BC dimer assembly (Fig. 3B) while the COMs of subunits A and B move further away by 4 Å. This unique LBD configuration in UBP301 with a partially formed BC dimer and desensitized-like monomeric state of subunits A and D points towards a weak LBD dimer interface in GluK3 and traps a state distinct from the UBP310 bound GluK3. This results in a non-classical arrangement of the LBDs in antagonist bound state. The entire set of four structures highlight the dynamics of the GluK3 receptors, especially with respect to the LBD domain.

2.5. Asp759 influences the stability of ligand binding domain dimers

One of the reasons for the weak LBD dimer interface could be Asp759, which is unique to GluK3 and is positioned near Asp730 from the other protomer in the 2-fold symmetric dimer interface. In order to test if Asp759 contributes to destabilizing the LBD dimer interface, we carried out atomistic molecular dynamics simulations of the wild-type LBD dimer and LBD dimer with Asp759Gly mutation in the presence of 150 mM NaCl. We measured the separation of the S1-S1 lobe that is linked to dimer stability and ultimately to the desensitization property of the receptor. Our results show that the S1-S1 equilibrium distance distribution in the wild-type LBD dimer is broad and varies from ~22–29 Å. In contrast, for the mutant Asp759Gly LBD dimer, the S1-S1 distance distribution is much narrower and ranges from ~18–22 Å (Fig. 3C). Our results suggest a

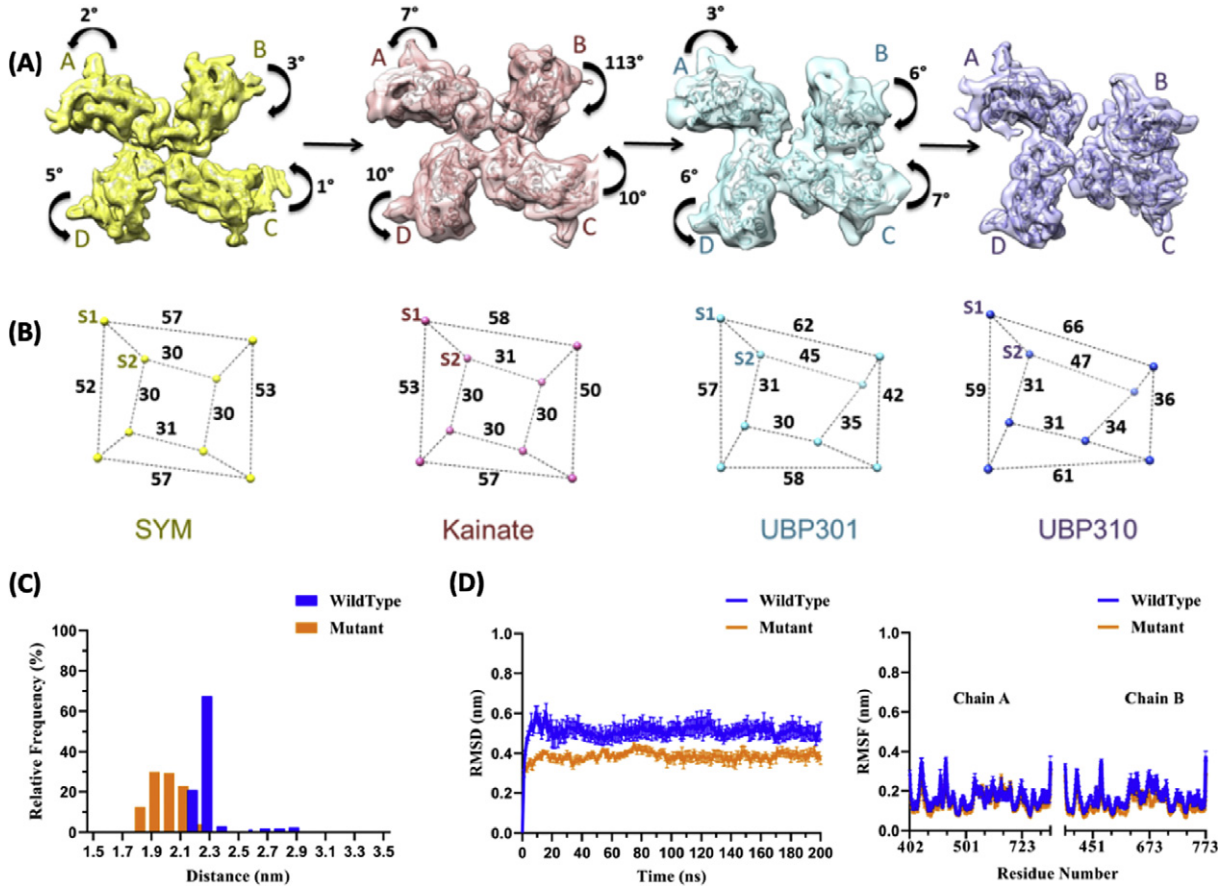

Fig. 3. Conformational changes at the LBD domain underlying receptor transitions between different states. (A) Top views of the segmented density maps for LBD fitted with coordinates shown in ribbon for SYM (6JFY), Kainate, UBP301 and UBP310 (6JFZ) bound states. Structural changes for the LBD tetramer underlying the transitions between various states is depicted. Degree and direction of LBD rotations are measured and indicated. (B) Distances from the centre of mass (spheres) between LBD S1 & S2 lobes are measured and indicated by dashed lines to highlight the domain movements. (C) Relative frequency histogram of S1-S1 distances between the wild type (blue) and mutant (orange) homo-dimers of LBD. A binning distance of 0.05 nm is used. (D) RMSD and RMSF plots of the backbone of LBD along with the standard error. RMSD and RMSF values for wild type receptor and mutant are in blue and orange.

tighter packing and increased stability of the LBD dimer in Asp759Gly mutant compared to wild-type (Fig. 3D). Analysis of the radius of gyration also shows that the mutant dimer is more compact compared to wild type protein (Supplementary Fig. S11). The increased stability of the dimer interface would lead to slower desensitization. Indeed, it has been shown previously *via* electrophysiological assays that GluK3 Asp759Gly mutant receptors desensitize with a Tau (des) of 18.4 ± 1.8 ms compared to wild-type which has Tau (des) of 5.0 ± 0.2 ms consistent with our simulations [10].

2.6. Apo-state GluK3 exhibits heterogeneity of the ligand-binding domains

The weaker, LBD dimer interface is likely to result in increased heterogeneity of the receptor in the apo state where the LBD domains are not stabilized by the ligands. To test this, we imaged GluK3 receptors in the apo state. To capture GluK3 in apo-state, we carried out negative stain analysis on purified apo-GluK3$_{EM}$ protein. The negative stain data reconstructions show that in the apo state, too, classical three-layered architecture *i.e.*, ATD-LBD-TM is maintained by the receptor. Consistent with our hypothesis, 2D classes reveal significant heterogeneity at the LBD layer to the extent that 3D reconstruction of the entire receptor was not possible (Fig. 4A). Due to the conformational heterogeneity of LBDs, their densities are not observed in the 3D map reconstruction (Fig. 4B). Nonetheless, the 2D classification and 3D reconstruction further reinforces the presence of an inherently weaker LBD dimer interface in GluK3 receptors compared to GluK2 or GluA2 receptors.

3. Discussion

Gating kinetics of iGluRs is the consequence of ligand binding that leads to structural rearrangements occurring in these receptors [20]. Understanding these transitions becomes conceivable when structural information about the receptor is obtained while trapped in different states. Previously crystal structures of individual domains of GluK3 in different states have been reported. However, the consequences of agonist and antagonist bound to these domains, on the complete receptor organization and thus its behavior were not clear. Besides, crystal structures come with constraints occurring due to lattice contacts [21]. Single-particle cryo-EM enables us to overcome these problems by imaging receptors in solution, free to adopt random orientations and conformations. In this study, we report structures of rat GluK3 receptor in agonist kainate and antagonist UBP301 bound states and compare it with existing full-length receptor structures to delineate conformational changes underlying receptor transitions. Kainate receptors swiftly undergo almost complete desensitization post agonist binding. While only subtle structural changes are observed at the ATD level in order to undergo a transition from the desensitized to closed state [13], major rearrangements happen at LBD with TM domains remaining in a closed-pore configuration (Supplementary Fig. 8). It is interesting to note that for homomeric GluK2-Kainate receptors, it has been shown that in the presence of Na^+ ions the LBD dimer interface is coupled in all the three states *viz*. the apo, antagonist-bound and activated (open channel) states while it gets decoupled only in the desensitized state [22]. Consistent with this, GluK2 structure in the antagonist bound state has the classical arrangement of LBDs as two dimers with 2-fold

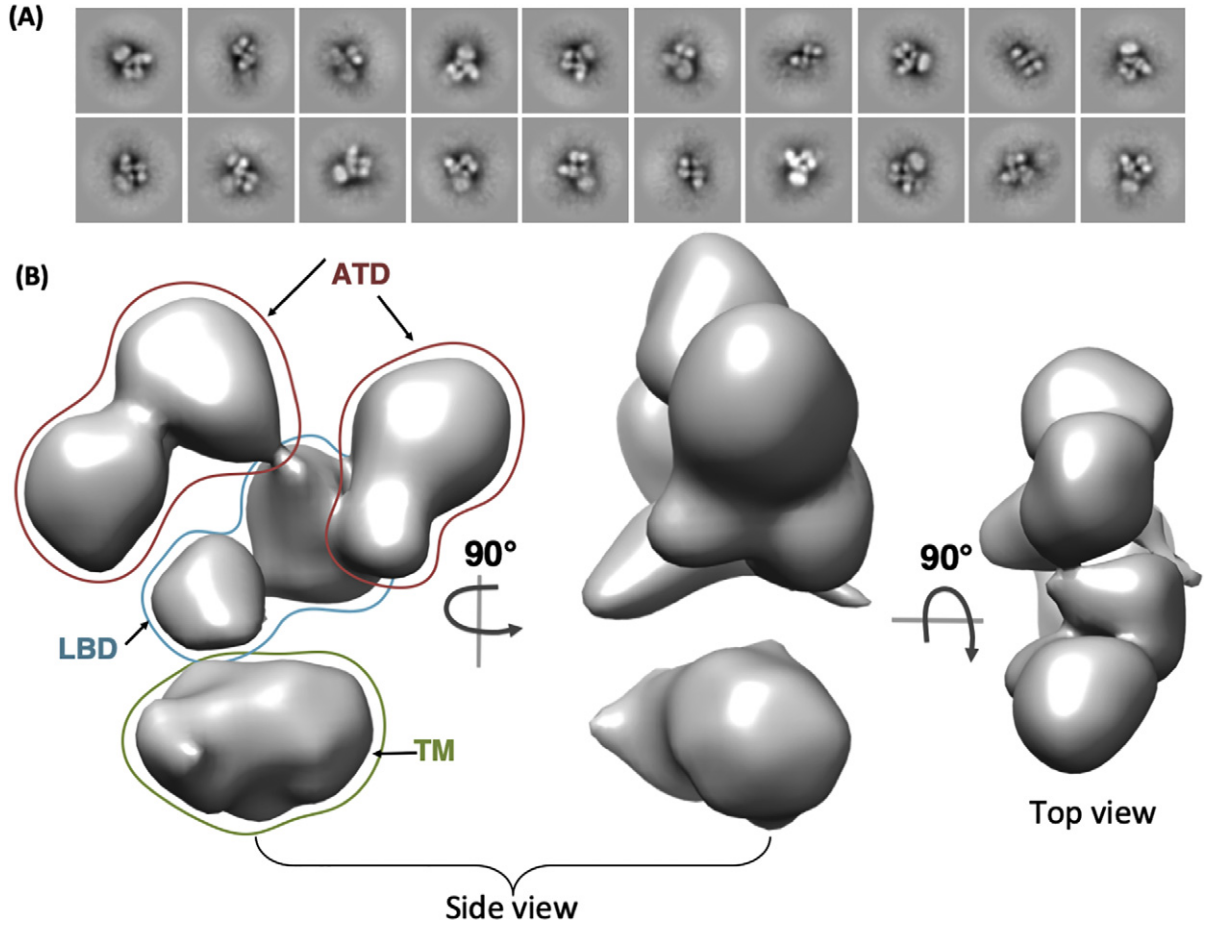

Fig. 4. Ligand Binding domain exhibits substantial heterogeneity in ligand free apo state. (A) Representative 2D classes from reference free 2D classification of negatively stained GluK3 receptors in apo state are shown. (B) Side and top views of *ab initio* 3D reconstruction from ~15,000 particles for apo-GluK3 is shown indicating poor density at the LBD domain likely due to conformational heterogeneity.

symmetric dimer and dimer-of-dimer interface, while the agonist bound state reveals LBDs in quasi-4-fold symmetric arrangement [18]. Single molecule fluorescence based studies in full-length GluK2 receptors also show a coupled LBD dimer interface in apo and antagonist bound states [22]. In contrast, our work provides evidence that GluK3 receptors have a much weaker dimer interface owing to which the classical LBD arrangement representative of resting/antagonist bound closed state is not observed. In both the UBP301 and UBP310 bound structures, only two LBD subunits were in partial-dimeric or dimeric arrangement. This weak dimer interface is consistent with faster desensitization and lower glutamate sensitivity of GluK3 receptors compared to that of GluK2 [23] [24]. Consistent with this, the apo receptors display significant heterogeneity. We further show by molecular dynamics simulations that one of the reasons could be attributed to residue Asp759 in GluK3 that lies at the LBD dimer interface and faces Asp730 on the formation of LBD dimer. This close apposition of two similarly charged residues likely induces a destabilization of the dimer interface by electrostatic repulsion generating fast desensitization properties. These charges are neutralized, and the LBD dimer interface is thus stabilized by binding of a Zn^{2+} ion which in turn potentiates current as reported earlier [10].

In conclusion, our work highlights the structural dynamics of GluK3 receptors and suggests that the unique properties of GluK3 receptors like fast desensitization, and low agonist sensitivity could be attributed to the weaker LBD dimer interface. Our study also helps to associate decades of electrophysiology based functional assays and biochemistry with receptor structure. This could prove useful in developing novel tools to target GluK3 containing kainate receptors therapeutically.

4. Materials and methods

4.1. Materials

All chemical reagents were purchased from Sigma-Aldrich, India. The DNA manipulation enzymes were from New England Biolabs. The pEGBacMam vector was a kind gift from Dr. Eric Gouaux. Detergents were purchased from Anatrace and ligands were obtained from Tocris.

4.2. GluK3 expression, detergent screening, and purification

As reported earlier, for improved and stable recombinant expression of GluK3, certain modifications were necessary for the wild type sequence resulting in $GluK3_{EM}$ construct [13] that was cloned into pEGBacMam vector [25]. To enhance the expression in HEK293 $GnTI^{-}$ cells, different concentrations of sodium butyrate were screened at 30 °C and 37 °C using Fluorescence detection Size Exclusion Chromatography (FSEC). Different detergents (DM, NDM, BOG, DDM, MNG, and DDM-CHS) were also screened to check recombinant protein stability at 4 °C. All the detergents for receptor solubilization were used at concentrations ~10 times of the reported CMC.

Based on expression optimization experiments, 10 mM sodium butyrate was added to the culture flasks after 20 h of infection and transferred to 30 °C for large-scale protein expression. Cells were harvested 60–70 h post-infection and re-suspended in ice-cold buffer containing 150 mM NaCl, 20 mM Tris (pH 8.0) and protease inhibitor cocktail. The re-suspended cells were disrupted by ultrasonication [QSonica sonicator, 4 cycles of 90 s] with constant stirring. The lysate was clarified by low-speed centrifugation, and membranes were collected by ultracentrifugation (37,000 rpm, 60 min). GluK3 protein was extracted from membrane fraction by solubilization with 0.75% w/v *n*-dodecyl-β-D-maltopyranoside (DDM), 0.005% w/v cholesterol hemisuccinate (CHS) in 150 mM NaCl, 20 mM Tris (pH 8.0) and purified by using cobalt-charged TALON metal affinity resin at 4 °C. Peak fractions were digested with thrombin at 1:100 wt/wt ratios. GluK3 receptor tetramers were isolated by size exclusion chromatography (Superose 6 10/300) in a buffer containing 150 mM NaCl, 20 mM Tris (pH 8.0), 0.75 mM DDM, and 0.02 mM CHS, concentrated to ~1.7 mg/mL (MWCO 100 kDa). Desensitized and closed states were trapped using 10 mM kainate, and 100 μM UBP301 respectively. The stability of the ligand bound protein was checked using FSEC.

4.3. Electron microscopy specimen preparation, data collection, and processing

Ligand free apo receptor was stained with uranyl acetate for negative-stain electron microscopy on carbon-coated copper grids whereas ligand complexed proteins were vitrified on quantifoil R1.3/1.2 Au 300 mesh grids for cryo-electron microscopy using an early prototype of VitroJet [26]. The negative stain grids for GluK3 apo were imaged using T12 microscope operated at a voltage of 120 kV. A total of 1215 micrographs were collected, and 39,912 particles were picked using Relion 2.1 [27] and exported to cryoSPARC [28]. After several rounds of data cleanup, the final 2D-classification was performed on 15,217 particles. These particles were further processed by following the *ab initio* reconstruction and homogeneous refinement as implemented in cryoSPARC. Cryo-EM datasets were collected on a Tecnai Arctica 200 kV microscope equipped with a Falcon 3 direct electron detection camera. A total of 2845 and 2005 movies were collected for GluK3-Kainate and GluK3-UBP301 complexes, respectively, at different defocus values in integrated mode. Motion correction and dose weighting were carried out using UCSF MOTIONCOR2 [29], and contrast transfer function (CTF) was estimated using CTFFIND4 [30] for each summed micrograph. Initially, ~1000 particles were picked manually and subjected to reference-free 2D classification in cryoSPARC V2. 2D classes from manually picked particles were used as a reference for auto picking from entire micrograph sets. A total of 124,268 and 118,670 particles were picked for GluK3-Kainate and GluK3-UBP301, respectively. Final 3D classification and reconstruction were performed in C1 symmetry on 46,106, and 24,997 particles for Kainate and UBP301 bound receptors, respectively. Refinement focused on the individual domains of their combinations didn't improve the map quality significantly.

4.4. Model building

GluK3-SYM (6JFY) and GluK3-UBP310 (6JFZ) [13] models as a template, were rigid-body fitted into cryo-EM density map of GluK3-Kainate and GluK3-UBP301 using UCSF-Chimera. To improve the fit, molecular dynamics based flexible fitting into the EM map was carried out using Namdinator [31]. The models were subjected to real space refinement using Phenix refine 1.15.2.3472 [32] and Coot 0.8.9.1 programs [33]. The quality and overall geometry of the structures was adjudged *via* Molprobity [34], and the structures were visualized and analyzed using PyMOL [35] and UCSF-Chimera [36].

4.5. Molecular dynamics simulations

The LBD dimer from GluK3-UBP310 (PDB ID: 6JFZ) was chosen as the initial model for atomistic molecular dynamics simulations. The LBD dimers with Asp759 in both monomers is referred to as wild type, while the dimers where Asp759 on both the subunits is mutated to glycine is referred to as mutant. LBDs in their homo-dimeric form were solvated using the TIP3P water model and neutralized with a 150 mM concentration of sodium and chloride ions. The system parameters were obtained from the CHARMM36 forcefield [37]. The minimum distance of solute from box edge is 1.0 nm. The potential energy of systems was minimized using 50,000 steps of steepest descent algorithm, followed by an equilibration phase of 100 ps in NVT and 2 ns in NPT ensembles. The final volume of the system is 115,201.0688 nm^3. Three independent runs of 200 ns each were performed for the wild type and mutant proteins using GROMACS 5.0.4 [38]. The temperature was maintained at 300 K using Nosé Hoover thermostat [39], and the pressure

was kept constant at 1 bar using the Parrinello-Rahman isotropic coupling scheme [40]. Long-range electrostatic interactions were calculated using the Particle Mesh Ewald method [41]. The analysis was done using tools of GROMACS and VMD [42]. For distance calculations, S1 is defined as the center of mass of residues Tyr513, Arg514, Lys515, Glu708, Ser709, and Thr710 [43].

4.6. Whole-cell voltage-clamp recordings

We evaluated the response of $GluK3_{EM}$ construct to ligands kainate and UBP301 using whole-cell patch-clamp as described earlier [13]. Briefly, human embryonic kidney 293 T (HEK 293T) cells were cultured on coverslips and either infected with $GluK3_{EM}$ baculovirus or transiently transfected with wild type receptors along with GFP expressing plasmid using Xfect reagent (Clontech). Currents were recorded from medium-sized cells at 48 to 60 h post-transfection. Whole-cells were lifted, and voltage was clamped at −80 mV using a HEKA USB 10 amplifier. Cells were bathed with extracellular solutions (ECS) containing NaCl (150 mM), KCl (2.8 mM), HEPES (10 mM), and $CaCl_2$ (0.5 mM), pH 7.3. Recording pipettes were pulled (Sutter, P-1000) from borosilicate glass capillaries (1.5 OD × 1.17 × 100 L mm, Harvard Apparatus). Pipette was filled with intracellular solution (ICS) containing CsCl (30 mM), CsF (100 mM), NaCl (4 mM), HEPES (10 mM), EGTA (5 mM), Na_2ATP (2 mM) and $CaCl_2$ (0.5 mM), pH 7.2. Currents were elicited by ultrafast ligand application for 200 ms *via* two-barrel theta pipette ultra-fast perfusion system mounted on a piezoelectric device (Multichannel Systems) controlled by Patchmaster software (HEKA) [44]. The current was filtered at 3 kHz and recorded at 20 kHz frequency. The whole cell recordings were accomplished using Patchmaster V2 × 90.2 (Heka Elektronick). Raw data files were analyzed using Igor Pro (ITX). In the presence of ligand, the desensitization kinetics were fitted by using pClamp 10.3 (Molecular Devices, US) exponential, standard method 2-term fitting (Levenberg-Marquard). Values are reported as Mean ± SEM. Statistical tests were performed in Prism.

Data availability

The cryo-EM density reconstructions and final models were deposited with the Electron Microscopy Data Base (accession code EMD-0790 and EMD-0839) and with the Protein Data Bank (accession code 6KZM, 6L6F). All other relevant data supporting the key findings of this study are available within the article and its Supplementary Information files or from the corresponding author upon request.

Authors' contribution

The project was conceptualized, designed, and monitored by JK. Jyoti Kumari carried out molecular biology, protein biochemistry, and EM analysis with assistance from JK and RBGR. RV performed electrophysiology experiments. RBGR collected the EM datasets. PJP provided resources for EM experiments and intellectual inputs at various stages. SB performed MD simulations under the guidance of MJ. ADB, JK, APB and JK integrated and analyzed all the data and prepared the manuscript with inputs from all the authors. All authors approved the final draft.

CRediT authorship contribution statement

Jyoti Kumari: Investigation, Writing - original draft. **Ameya D. Bendre:** Formal analysis, Visualization, Writing - original draft. **Sumedha Bhosale:** Investigation. **Rajesh Vinnakota:** Investigation. **Ananth P. Burada:** Data curation, visualization. **Giancarlo Tria:** Investigation. **Raimond B.G. Ravelli:** Investigation, Resources. **Peter J. Peters:** Resources, Methodology. **Manali Joshi:** Investigation, Formal analysis, Visualization, Supervision. **Janesh Kumar:** Conceptualization, Methodology, Supervision, Funding acquisition, Writing - review & editing.

Acknowledgment

The research program in our laboratory is supported by the Wellcome Trust DBT India Alliance (IA/I/13/2/501023) and Centre of Excellence grant BT/PR15450/COE/34/46/2016 from Department of Biotechnology, India. Jyoti Kumari thanks University Grants Commission, India for senior research fellowship. R.V. is supported by SERB-N-PDF fellowship (N-PDF/2016/002621). A.D.B is supported by a research associate fellowship by DBT, India. We thank Frank Nijpels for EM grid vitrification. We also acknowledge the help of Giancarlo Tria and Abril Gijsbers in the extensive screening of suitable conditions for cryo and negative stain grid preparation. We thank Dr. Carmen Lopez-Iglesias and microscopy core lab team at M4I for facilitating this work. Dr. Mark L. Mayer kindly gifted the various iGluR constructs that were sub-cloned and used for construct optimization and mutational studies. Dr. Eric Gouaux kindly provided the pEGBacMam vector.

Declaration of competing interest

The authors declare no competing interests.

Appendix A. Supplementary data

Supplementary data to this article can be found online at https://doi.org/10.1016/j.ijbiomac.2020.01.282.

References

[1] J. Lerma, J.M. Marques, Kainate receptors in health and disease, Neuron 80 (2013) 292–311.
[2] F. Stephen, T. LPW, C.J. McBain, F.S. Menniti, K.M. Vance, K.K. Ogden, K.B. Hansen, H. Yuan, S.J. Myers, R. Dingledine, Glutamate receptor ion channels: structure, regulation, and function, Pharmacol. Rev. 62 (2010) 405–496.
[3] A.V. Paternain, A. Cohen, Y. Stern-Bach, J. Lerma, A role for extracellular Na + in the channel gating of native and recombinant Kainate receptors, J. Neurosci. 23 (2018) 8641–8648.
[4] P.S. Pinheiro, C. Mulle, Presynaptic glutamate receptors: physiological functions and mechanisms of action, Nat. Rev. Neurosci. 9 (2008) 423–436.
[5] J.D. Shepherd, R.L. Huganir, The cell biology of synaptic plasticity: AMPA receptor trafficking, Annu. Rev. Cell Dev. Biol. 23 (2007) 613–643.
[6] D. Bowie, Ionotropic glutamate receptors & CNS disorders, CNS Neurol. Disord. Drug Targets 7 (2008) 129–143.
[7] A. Dutta, J. Krieger, J.Y. Lee, J. Garcia-Nafria, I.H. Greger, I. Bahar, Cooperative dynamics of intact AMPA and NMDA glutamate receptors: similarities and subfamily-specific differences, Structure 23 (2015) 1692–1704.
[8] P.S. Pinheiro, D. Perrais, F. Coussen, J. Barhanin, B. Bettler, J.R. Mann, J.O. Malva, S.F. Heinemann, C. Mulle, GluR7 is an essential subunit of presynaptic kainate autoreceptors at hippocampal mossy fiber synapses, Proc. Natl. Acad. Sci. U. S. A. 104 (2007) 12181–12186.
[9] D. Perrais, F. Coussen, C. Mulle, Atypical functional properties of GluK3-containing kainate receptors, J. Neurosci. 29 (2009) 15499–15510.
[10] J. Veran, J. Kumar, P.S. Pinheiro, A. Athané, M.L. Mayer, D. Perrais, C. Mulle, Zinc potentiates GluK3 glutamate receptor function by stabilizing the ligand binding domain dimer interface, Neuron 76 (2012) 565–578.
[11] R. Venskutonyte, K. Frydenvang, M. Gajhede, L. Bunch, D.S. Pickering, J.S. Kastrup, Binding site and interlobe interactions of the ionotropic glutamate receptor GluK3 ligand binding domain revealed by high resolution crystal structure in complex with (S)-glutamate, J. Struct. Biol. 176 (2011) 307–314.
[12] J. Kumar, M.L. Mayer, Crystal structures of the glutamate receptor ion channel GluK3 and GluK5 amino-terminal domains, J. Mol. Biol. 404 (2010) 680–696.
[13] J. Kumari, R. Vinnakota, J. Kumar, Structural and functional insights into GluK3-kainate receptor desensitization and recovery, Sci. Rep. 9 (2019), 10254.
[14] H.H. Schiffer, G.T. Swanson, S.F. Heinemann, Rat GluR7 and a carboxy-terminal splice variant, GluR7b, are functional kainate receptor subunits with a low sensitivity to glutamate, Neuron 19 (1997) 1141–1146.
[15] S.H.W. Scheres, S. Chen, Prevention of overfitting in cryo-EM structure determination, Nat. Methods 9 (2012) 853–854.
[16] K.L. Dürr, L. Chen, R.A. Stein, R. De Zorzi, I.M. Folea, T. Walz, H.S. Mchaourab, E. Gouaux, Structure and Dynamics of AMPA Receptor GluA2 in Resting, Pre-Open, and Desensitized States, Cell 158 (2014) 778–792.
[17] E. Gouaux, A.I. Sobolevsky, M.P. Rosconi, X-ray structure, symmetry and mechanism of an AMPA-subtype glutamate receptor, Nature 462 (2009) 745–756.
[18] J.R. Meyerson, J. Kumar, S. Chittori, P. Rao, J. Pierson, A. Bartesaghi, M.L. Mayer, S. Subramaniam, Structural mechanism of glutamate receptor activation and desensitization, Nature 514 (2014) 328–334.
[19] J.R. Meyerson, S. Chittori, A. Merk, P. Rao, T.H. Han, M. Serpe, M.L. Mayer, S. Subramaniam, Structural basis of kainate subtype glutamate receptor desensitization, Nature 537 (2016) 567–571.

[20] K. Raymond Dingledine, The glutamate receptor ion channels, Pharmacol. Rev. 51 (1999) 7–61.
[21] K.R. Acharya, M.D. Lloyd, The advantages and limitations of protein crystal structures, Trends Pharmacol. Sci. 26 (2005) 10–14.
[22] D.B. Litwin, E. Carrillo, S.A. Shaikh, V. Berka, V. Jayaraman, The structural arrangement at intersubunit interfaces in homomeric kainate receptors, Sci. Rep. 9 (2019) 6969.
[23] D. Perrais, J. Veran, C. Mulle, Gating and permeation of kainate receptors: differences unveiled. Trends Pharmacol. Sci. 11 (2010) 516–522.
[24] B. Bettler, J. Egebjerg, G. Sharma, G. Pecht, I. Hermans-Borgmeyer, C. Moll, C.F. Stevens, S. Heinemann, Cloning of a putative glutamate receptor: a low affinity kainate-binding subunit, Neuron 8 (1992) 257–265.
[25] A. Goehring, C.H. Lee, K.H. Wang, J.C. Michel, D.P. Claxton, I. Baconguis, T. Althoff, S. Fischer, K.C. Garcia, E. Gouaux, Screening and large-scale expression of membrane proteins in mammalian cells for structural studies, Nat. Protoc. 9 (2014) 2574–2585.
[26] R.B.G. Ravelli, F.J.T. Nijpels, R.J.M. Henderikx, G. Weissenberger, S. Thewessem, A. Gijsbers, B.W. Beulen, C. Lopez-Iglesias, P. Peters, Automated cryo-EM sample preparation by pin-printing and jet vitrification, bioRxiv (2019) https://doi.org/10.1101/651208.
[27] S.H.W. Scheres, RELION: implementation of a Bayesian approach to cryo-EM structure determination, J. Struct. Biol. 180 (2012) 519–530.
[28] A. Punjani, J.L. Rubinstein, D.J. Fleet, M.A. Brubaker, CryoSPARC: algorithms for rapid unsupervised cryo-EM structure determination, Nat. Methods 14 (2017) 290–296.
[29] H. Peng, Z. Zhou, E. Meijering, T. Zhao, G.A. Ascoli, M. Hawrylycz, MotionCor2: anisotropic correction of beam-induced motion for improved cryo-electron microscopy, Nat. Methods 14 (2017) 332–333.
[30] A. Rohou, N. Grigorieff, CTFFIND4: fast and accurate defocus estimation from electron micrographs, J. Struct. Biol. 192 (2015) 216–221.
[31] R.T. Kidmose, J. Juhl, P. Nissen, T. Boesen, J.L. Karlsen, B.P. Pedersen, Namdinator – automatic molecular dynamics flexible fitting of structural models into cryo-EM and crystallography experimental maps, IUCrJ 6 (2019) 526–531.
[32] P.V. Afonine, B.K. Poon, R.J. Read, O.V. Sobolev, T.C. Terwilliger, A. Urzhumtsev, P.D. Adams, Real-space refinement in PHENIX for cryo-EM and crystallography, Acta Crystallographica Section D: Structural Biology 74 (2018) 531–544.
[33] P. Emsley, K. Cowtan, Coot: model-building tools for molecular graphics, Acta Crystallogr. D Biol. Crystallogr. 60 (2004) 2126–2132.
[34] I.W. Davis, A. Leaver-Fay, V.B. Chen, J.N. Block, G.J. Kapral, X. Wang, L.W. Murray, I.I.I.W.B. Arendall, J. Snoeyink, J.S. Richardson, et al., MolProbity: all-atom contacts and structure validation for proteins and nucleic acids, Nucleic Acids Res. 35 (2007) W375–W383.
[35] WL Delano, The PyMOL Molecular Graphics System, Schrodinger, 2002. http://www.pymol. sourceforge.net.
[36] E.F. Pettersen, T.D. Goddard, C.C. Huang, G.S. Couch, D.M. Greenblatt, E.C. Meng, T.E. Ferrin, UCSF chimera? A visualization system for exploratory, J. R. Soc. Interface 8 (2004) 1605–1612.
[37] P. Bjelkmar, P. Larsson, M.A. Cuendet, B. Hess, E. Lindahl, Implementation of the CHARMM force field in GROMACS: analysis of protein stability effects from correction maps, virtual interaction sites, and water models, J. Chem. Theory Comput. 6 (2010) 459–466.
[38] S. Pronk, S. Páll, R. Schulz, P. Larsson, P. Bjelkmar, R. Apostolov, M.R. Shirts, J.C. Smith, P.M. Kasson, D. van der Spoel, B. Hess, E. Lindahl, GROMACS 4.5: a high-throughput and highly parallel open source molecular simulation toolkit, Bioinformatics 29 (2013) 845–854.
[39] G.J. Martyna, M.L. Klein, M. Tuckerman, Nosé–hoover chains: the canonical ensemble via continuous dynamics, J. Chem. Phys. 97 (1992) 2635–2643.
[40] M. Parrinello, A. Rahman, Polymorphic transitions in single crystals: a new molecular dynamics method, J. Appl. Phys. 52 (1981) 7182–7190.
[41] U. Essmann, L. Perera, M.L. Berkowitz, T. Darden, H. Lee, L.G. Pedersen, A smooth particle mesh Ewald method, J. Chem. Phys. 103 (1995) 8577–8593.
[42] W. Humphrey, A. Dalke, K. Schulten, VMD: visual molecular dynamics, J. Mol. Graph. 14 (1996) 33–38.
[43] T. Paramo, P.M.G.E. Brown, M. Musgaard, D. Bowie, P.C. Biggin, Functional validation of Heteromeric Kainate receptor models, Biophys. J. 113 (2017) 2173–2177.
[44] A. Brüggemann, C. Farre, C. Haarmann, A. Haythornthwaite, M. Kreir, S. Stoelzle, M. George, N. Fertig, Planar patch clamp: advances in electrophysiology, Methods Mol. Biol. 491 (2008) 165–176.